Mechanism of RNA polymerase II stalling by DNA alkylation

Stefano Malvezzi[a,1], Lucas Farnung[b,1], Claudia M. N. Aloisi[a], Todor Angelov[a], Patrick Cramer[b,2], and Shana J. Sturla[a,2]

[a]Department of Health Sciences and Technology, ETH Zurich, 8092 Zurich, Switzerland; and [b]Max Planck Institute for Biophysical Chemistry, 37077 Göttingen, Germany

Edited by Graham C. Walker, Massachusetts Institute of Technology, Cambridge, MA, and approved September 26, 2017 (received for review May 3, 2017)

Several anticancer agents that form DNA adducts in the minor groove interfere with DNA replication and transcription to induce apoptosis. Therapeutic resistance can occur, however, when cells are proficient in the removal of drug-induced damage. Acylfulvenes are a class of experimental anticancer agents with a unique repair profile suggesting their capacity to stall RNA polymerase (Pol) II and trigger transcription-coupled nucleotide excision repair. Here we show how different forms of DNA alkylation impair transcription by RNA Pol II in cells and with the isolated enzyme and unravel a mode of RNA Pol II stalling that is due to alkylation of DNA in the minor groove. We incorporated a model for acylfulvene adducts, the stable 3-deaza-3-methoxynaphtylethyl-adenosine analog (3d-Napht-A), and smaller 3-deaza-adenosine analogs, into DNA oligonucleotides to assess RNA Pol II transcription elongation in vitro. RNA Pol II was strongly blocked by a 3d-Napht-A analog but bypassed smaller analogs. Crystal structure analysis revealed that a DNA base containing 3d-Napht-A can occupy the +1 templating position and impair closing of the trigger loop in the Pol II active center and polymerase translocation into the next template position. These results show how RNA Pol II copes with minor-groove DNA alkylation and establishes a mechanism for drug resistance.

transcription | DNA alkylation | RNA polymerase II | polymerase stalling | drug resistance

The catalysis of transcription by RNA polymerase is fundamental to the viability of growing cells. In conventional cancer chemotherapy, DNA damage products that interfere with genomic processes initiate cell death. However, therapeutic resistance of cancer cells to DNA alkylating agents may result when cells are proficient in the repair of drug-induced damage (1–3). Acylfulvenes (AFs) are a class of experimental anticancer drugs that appear to be selectively repaired by the transcription-coupled subpathway of nucleotide excision repair (TC-NER) (4–6). Thus, AF-induced DNA adducts are preferentially removed from actively transcribed regions of the genome but are largely ignored by global-genome repair. These findings suggest that the AF-DNA adduct does not perturb the duplex structure yet impedes the progress of RNA polymerase. Understanding the chemical basis of how DNA alkylation stalls RNA polymerase to initiate repair can provide key insight for the design of therapeutics less prone to failure due to resistance.

AFs are semisynthetic derivatives of the fungal sesquiterpene illudin S and alkylate DNA in the minor groove (7), a common property for several anticancer agents such as distamycins, lexitropsins, duocarmycins, and ecteinascidin 743, as well as peptide-based minor-groove binders (8). Hydroxymethylacylfulvene (HMAF, irofulven) was tested previously in clinical trials for several cancers and is anticipated to reenter clinical trials with biomarker-driven patient stratification strategies (9). AFs are prodrugs that are reductively activated by prostaglandin reductase 1 (PTGR1) to alkylate primarily position 3 of adenine (7) (Fig. 1*A*). Inhibition of DNA synthesis and capacity to induce cell-cycle arrest of minor-groove alkylating agents is attributed primarily to alkylation of DNA, and levels of 3-AF-A in AF-treated cancer cells are proportional to cytotoxicity (7, 10–13).

Cells have evolved various DNA repair functions, and large helix-distorting adducts are often removed by NER. NER is divided into two subpathways: TC- and global genome- (GG-) NER (14). TC-NER–deficient human fibroblast cells are more sensitive to illudin S, AF, and HMAF compared with GG-NER–deficient human fibroblast cells, suggesting that TC-NER selectively repairs AF adducts (4–6) (Fig. 1*A*). Moreover, siRNA-mediated down-regulation of TC-NER in a cancer cell line greatly increased their sensitivity to AF, whereas down-regulation of GG-NER did not (6) (Fig. 1*A*). Since AF adducts are selectively repaired by TCR and ignored by GG-NER, a large portion of adducts that are not repaired in surviving cells are expected to be a basis of the increased mutation frequency observed in cell lines (15). Indeed, error-prone bypass of minor-groove modifications has been characterized for certain translesion synthesis DNA polymerases (16). Finally, exposing a cancer cell line to UCN-01, a compound that inhibits Chk1, enabling checkpoint evasion and reduction of NER function, increased sensitivity to AF and AF adducts persisted longer (12, 17). The repair and persistence profiles for AF-DNA adducts thus suggests that the basis of selective removal is associated with the DNA damage recognition step.

The main difference between the TC and GG subpathways of NER is the DNA damage recognition step: GG-NER is activated by XPC-RAD23B factors that sense the altered helix conformation induced by DNA damage, whereas TC-NER is activated

Significance

RNA polymerase II (Pol II) catalyzes the transcription of DNA to RNA in the nucleus. DNA alkylating cancer drugs can stall transcription; however, the basis for Pol II stalling when encountering a DNA template with minor-groove alkylation adducts has remained elusive due to its inherent chemical instability. We characterized the behavior of Pol II in transcription over minor-groove alkylation adducts and uncovered a previously unobserved mode of Pol II stalling wherein clashes between DNA adducts and the mobile trigger loop of RNA Pol II prevent translocation of the enzyme after nucleotide insertion. These results provide a molecular basis for how DNA damage in transcribed portions of the genome initiates DNA repair contributing to drug resistance.

Author contributions: S.M., L.F., C.M.N.A., T.A., P.C., and S.J.S. designed research; S.M., L.F., C.M.N.A., and T.A. performed research; S.M., L.F., and T.A. contributed new reagents/analytic tools; S.M., L.F., C.M.N.A., T.A., P.C., and S.J.S. analyzed data; and S.M., L.F., P.C., and S.J.S. wrote the paper.

The authors declare no conflict of interest.

This article is a PNAS Direct Submission.

Data deposition: The atomic coordinates and structure factors have been deposited in the Protein Data Bank, www.wwpdb.org (PDB ID code 5OT2).

[1]S.M. and L.F. contributed equally to this work.

[2]To whom correspondence may be addressed. Email: patrick.cramer@mpibpc.mpg.de or sturlas@ethz.ch.

This article contains supporting information online at www.pnas.org/lookup/suppl/doi:10.1073/pnas.1706592114/-/DCSupplemental.

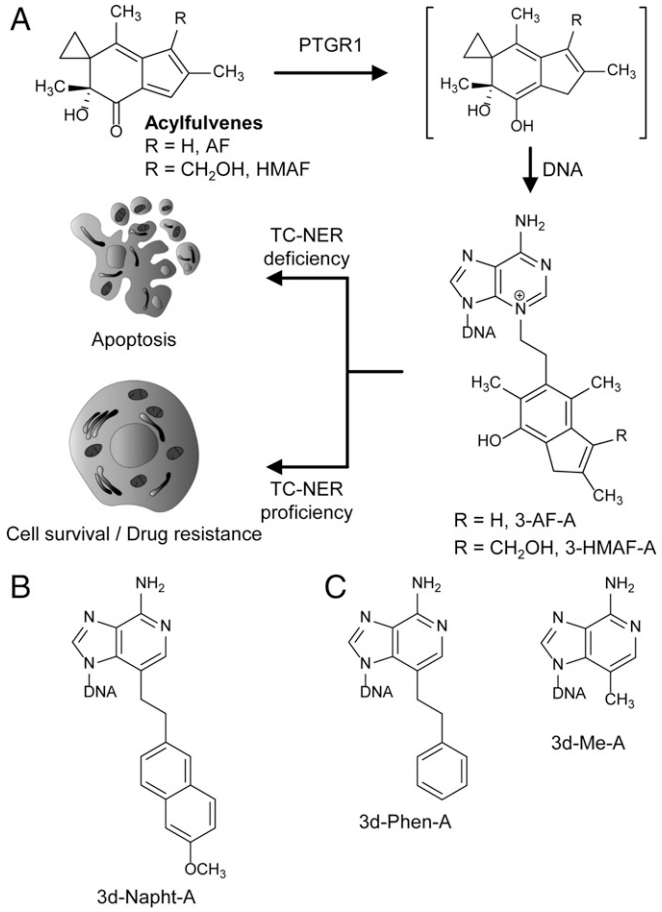

Fig. 1. DNA alkylation by AFs and structures of minor-groove modifications. (*A*) Mechanism of AF activation, alkylation, and impact on cell viability depending on DNA repair proficiency. (*B*) The 3d-Napht-A analog as model of AF-derived DNA adducts. (*C*) 3-Deaza-adenosine analogs of decreasing size, 3d-Phen-A, and 3-Me-A for structure-activity analysis of Pol II bypass.

by the stalling of RNA polymerase II (Pol II) (14, 18). Therefore, a working hypothesis is that 3-AF-A stalls Pol II but does not induce significant helix distortion (6). Pol II efficiently transcribes over small DNA lesions like O^6-methyl-guanine (O^6-Me-G), 8-oxo-guanine, N2-1-carboxyethyl-guanine, and N3-carboxymethyl-thymine, among others (19–22); however, larger modifications can induce it to stall. Upon Pol II stalling, downstream factors are recruited to the damage site, and the repair process then progresses in the same manner as for GG-NER (14, 18).

The mechanism of Pol II stalling at several DNA lesions has been elucidated. Cyclobutane pyrimidine dimers, cisplatin 1,2-d(GPG) intrastrand cross-links, monofunctional pyriplatin-guanine adducts, and 8,5′-cyclo-2′-deoxyadenosine strongly inhibit Pol II progression, and crystal structures of yeast Pol II bound to DNA containing these lesions were solved to elucidate the basis of polymerase stalling or bypass (23–28). Two flexible elements of the Pol II active site, the bridge helix and the trigger loop, are required for nucleotide addition and nucleic acid translocation to the next template position (29–32). Wang and coworkers (33) reported the blockage of Pol II by minor-groove-binding pyrrole-imidazole polyamides and identified their interaction with the residues Arg1386 and His1387 in the conserved switch 1 region of Rpb1 by molecular modeling. Despite these insights, there is no direct observation of Pol II encountering a DNA template with minor-groove adducts, and it is unknown how Pol II deals with minor-groove-binding and -modifying agents.

In this study, the question of how minor-groove DNA alkylation impedes RNA synthesis was addressed. Evaluating transcription activity in a human cancer cell confirmed the inhibited RNA synthesis. Due to the chemical instability of the native AF adduct (7, 12), we characterized the behavior of Pol II in transcription over its stable analog 3-deaza-3-methoxynaphtylethyl-adenosine (3d-Napht-A) (16) (Fig. 1*B*). We tested the capacity of 3d-Napht-A to stall purified RNA Pol II with DNA constructs mimicking the transcription bubble and ternary elongation complexes (ECs) and tested the limits of Pol II's size tolerance of minor-groove alkyl adducts by carrying out the same investigation with other 3-deaza-alkyl-adenosine analogs of systematically smaller size [i.e., 3-deaza-3-phenethyl-adenosine (3d-Phen-A) and 3-deaza-3-methyl-adenosine (3d-Me-A)] (Fig. 1*C*). The mechanism of stalling was furthermore investigated by crystallographic analysis of the stalled Pol II in the ternary EC with bound DNA template and RNA transcript. These data reveal a previously unobserved mode of Pol II stalling and provide insights into the chemical topology of minor-groove modifications required to stall transcription in cancer cells.

Results

DNA Alkylation Impairs RNA Synthesis in Cells. It has been established that cells proficient in TC-NER are more resistant to cytotoxicity induced by AFs (4–6). To evaluate how AF impacts RNA synthesis in cancer cells relative to a simple methylating agent we compared RNA synthesis activity following treatment with HMAF vs. methylmethane sulfonate (MMS). MMS can form various DNA methylation adducts, mainly the noncytotoxic 7-Me-G, but also 3-Me-A, and to a lesser extent O^6-Me-G (34, 35). A significant reduction of RNA synthesis in colon adenocarcinoma SW480 cells overexpressing PTGR1 (SW480-PTGR1), an enzyme required for metabolic bioactivation of AFs, was observed after treatment with 1 μM HMAF, but not 1 μM MMS (Fig. S2), concentrations at which all cells remained viable (Fig. S1). Because MMS is much less potent than HMAF, we also evaluated RNA synthesis at doses that reduce cell viability equally with both compounds (Fig. S3). Again, RNA synthesis was significantly reduced in cells treated with 0.5 μM HMAF, but not in cells treated with 500 μM MMS. These results provide evidence for Pol II stalling after minor-groove DNA alkylation in cancer cells.

Pol II Transcription Can Stall at Minor-Groove Alkylation Adducts. With strong indication that AF-DNA damage stalls transcription in cells, we assessed directly the capacity of the major 3-AF DNA adduct to impede the progress of RNA Pol II using purified yeast Pol II and DNA that contains 3d-Napht-A, a chemically stable analog of the adduct (16), in constructs of a transcription bubble with 3d-Napht-A four bases downstream of the growing RNA 3′ end (36) (Fig. S4*A*). When RNA was extended in the presence of four NTPs, Pol II stalled after nucleotide incorporation opposite the 3d-Napht-A, whereas it transcribed efficiently over unmodified A or the smaller methylated analog 3d-Me-A (Fig. S4*B*). RNA extension of a transcription bubble with 3d-Napht-A nine bases downstream of the RNA 3′ end also behaved similarly (Fig. S4 *C* and *D*).

We next characterized RNA extension with ternary ECs composed of an RNA annealed to a DNA template containing the analog at the nucleotide incorporation site +1 (Fig. 2*A*). In the presence of all four NMPs, Pol II stalled at 3d-Napht-A after incorporating one NMP (Fig. 2*B*) and no bypass was observed even after 60 min. When the same reactions were carried out with individual nucleotides, Pol II incorporated UMP and misincorporated CMP opposite 3d-Napht-A but not GMP and AMP (Fig. 2*C*).

Pol II Is Tolerant to Smaller Modifications but Errors Arise. To derive the maximum adduct size tolerated by Pol II, RNA extension was evaluated for templates containing smaller alkyl groups. Pol II efficiently extended RNA annealed with templates containing A

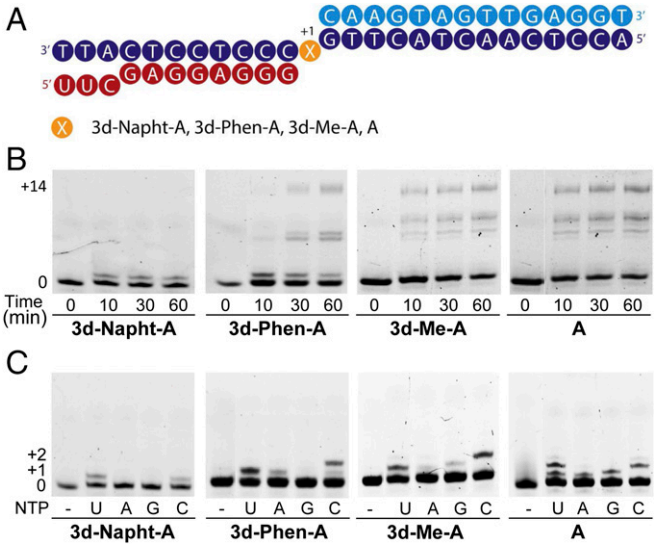

Fig. 2. Pol II full-length synthesis and single-nucleotide incorporation. (*A*) Ternary ECs containing A, 3d-Me-A, 3d-Phen-A, or 3d-Napht-A at the underlined position, used for primer extension reactions. DNA template is dark blue, nontemplate DNA is light blue, RNA primer is red. (*B*) Denaturing gel electrophoresis of Pol II transcription products in the presence of all four NTPs (1 mM). Extension of the RNA primer to the end of the DNA template forms the indicated run-off product (+14). (*C*) Single-nucleotide incorporation opposite A, 3d-Me-A, 3d-Phen-A, and 3d-Napht-A. Reactions were performed in presence of a single NTP (1 mM) and were quenched after 20 min.

or 3d-Me-A, forming full-length products (Fig. 2*B*). The 3d-Phen-A was bypassed, but product accumulated after incorporation of the first nucleotide, suggesting the intermediate-size adduct slows Pol II but does not impede it completely.

In the presence of individual nucleotides, UMP was very efficiently incorporated, leading to a +2 band resulting from insertion of UMP opposite A plus the next G. For modified substrates with 3d-Me-A or 3d-Phen-A, however, only the +1 band was observed for UMP, suggesting that the 3-alkyl groups reduced transcription fidelity. A similar degree of CMP misincorporation was observed in all cases, regardless of whether the DNA was modified or not (Fig. S5). Moreover, Pol II efficiently misincorporated CMP opposite the next templating G forming a +2 band product, whereas in the case of 3d-Napht-A only one nucleotide was inserted opposite the analog.

DNA Alkylation Alters Pol II Incorporation and Extension Efficiency. Having established that Pol II incorporates UMP and CMP to varying extents depending on the identity of DNA modification, we measured apparent reaction rates for their incorporation by Pol II (Fig. 3). For insertion of UTP opposite A or 3d-Me-A, incorporation rates were similar (9.0 ± 1.4 min^{-1} and 8.0 ± 1.2 min^{-1}, respectively), whereas rates opposite 3d-Phen-A and 3d-Napht-A were significantly reduced (2.5 ± 0.2 min^{-1} and 1.2 ± 0.2 min^{-1}, respectively). The CMP misincorporation profile was quite different, however, with more than 10-fold greater incorporation opposite 3d-Me-A vs. A (5.8 ± 0.4 min^{-1} vs. 0.5 ± 0.1 min^{-1}), whereas 3d-Phen-A and 3d-Napht-A were similarly low as A (0.28 ± 0.03 min^{-1} and 0.39 ± 0.05 min^{-1}) (Fig. 3*A*). The increased misincorporation of CMP opposite the 3-alkyl-adenosine analogs relative to A (Fig. 3*A*) suggests a potential basis of transcriptional mutagenesis in cells (21, 37).

To understand the impact of 3-deaza-3-alkyl-adenosine analogs on Pol II activity during the extension steps following incorporation opposite an adduct we evaluated RNA synthesis using DNA constructs with the RNA transcript containing either U or C opposite 3-deaza-3-alkyl-adenosine analogs and measured rates of CMP incorporation opposite the next templating G (Fig. 3*B*). Extension after 3d-Me-A was similar to after A, but after 3d-Phen-A extension from U or C was 170- or 250-fold lower, respectively, and after 3d-Napht-A extension by Pol II was totally blocked, with no incorporation even after 60 min. This observation was consistent with the initially observed stalling after insertion of one nucleotide opposite the modified base. From these data it could be concluded that Pol II is stalled by the larger analog 3d-Napht-A whereas it bypasses smaller analogs, with the efficiency decreasing in step with the size of the 3-alkyl group size. The efficient bypass of 3d-Me-A was consistent with the observation that exposing cells to MMS did not reduce transcription.

Structural Investigation of Pol II Stalling by DNA Alkylation. To investigate the mechanism of Pol II stalling opposite an alkylated template base we determined the structure of a Pol II EC in the presence of 3d-Napth-A. We reconstituted a 12-subunit *Saccharomyces cerevisiae* Poll II EC with a modified nucleic acid scaffold (Fig. 4*A*). The resulting complex was crystallized, and the structure was determined using molecular replacement. Electron density was observed for 8 bp of downstream DNA, for the DNA template strand up to upstream position −10, and for the entire RNA except for the 5′-terminal base at the upstream

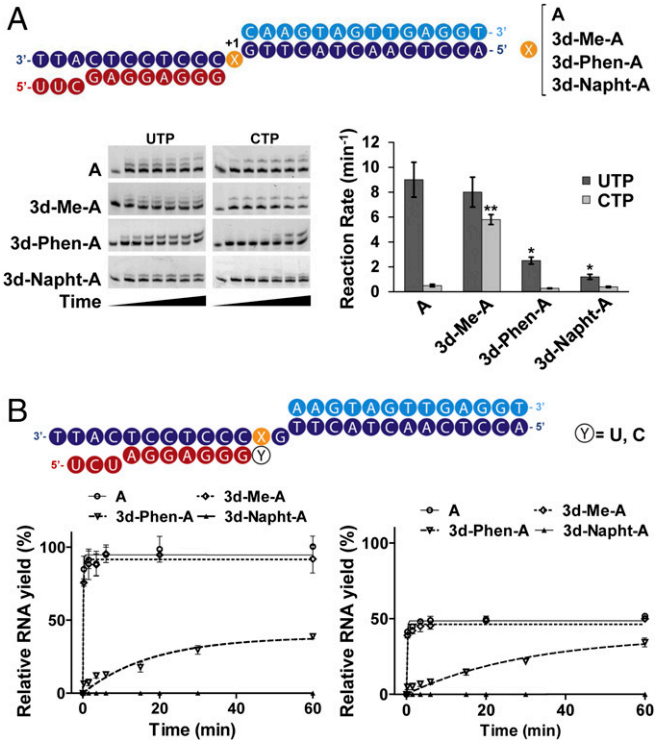

Fig. 3. Single-nucleotide incorporation and extension kinetics. (*A*) Gel denaturing electrophoresis of primer extension kinetics by Pol II for UMP and CMP incorporation opposite unmodified adenine or 3-deaza-adenosine analogs. Reactions contained 1 mM NTP and were stopped at various time points between 0 and 60 min. Schematic representation of apparent rate constants for UMP and CMP incorporation kinetics (*Right*). Error bars represent SD ($n = 3$) and statistical significance for NMP incorporation opposite the 3-deaza-3-alkyl-adenosine adducts compared with A was determined by unpaired Student *t* test with Welch's correction (*$P < 0.05$, **$P < 0.01$). (*B*) Rates (minutes^{-1}) of RNA primer extension from the correct base pair A_{analog}:U (*Left*) and the mismatched base pair A_{analog}:C (*Right*). The DNA template contained either A, 3d-Me-A, 3d-Phen-A, or 3d-Napht-A at the indicated position. RNA yield is plotted as a function of time (100% RNA yield corresponds to 50% of primer extension). Error bars represent SD ($n = 3$).

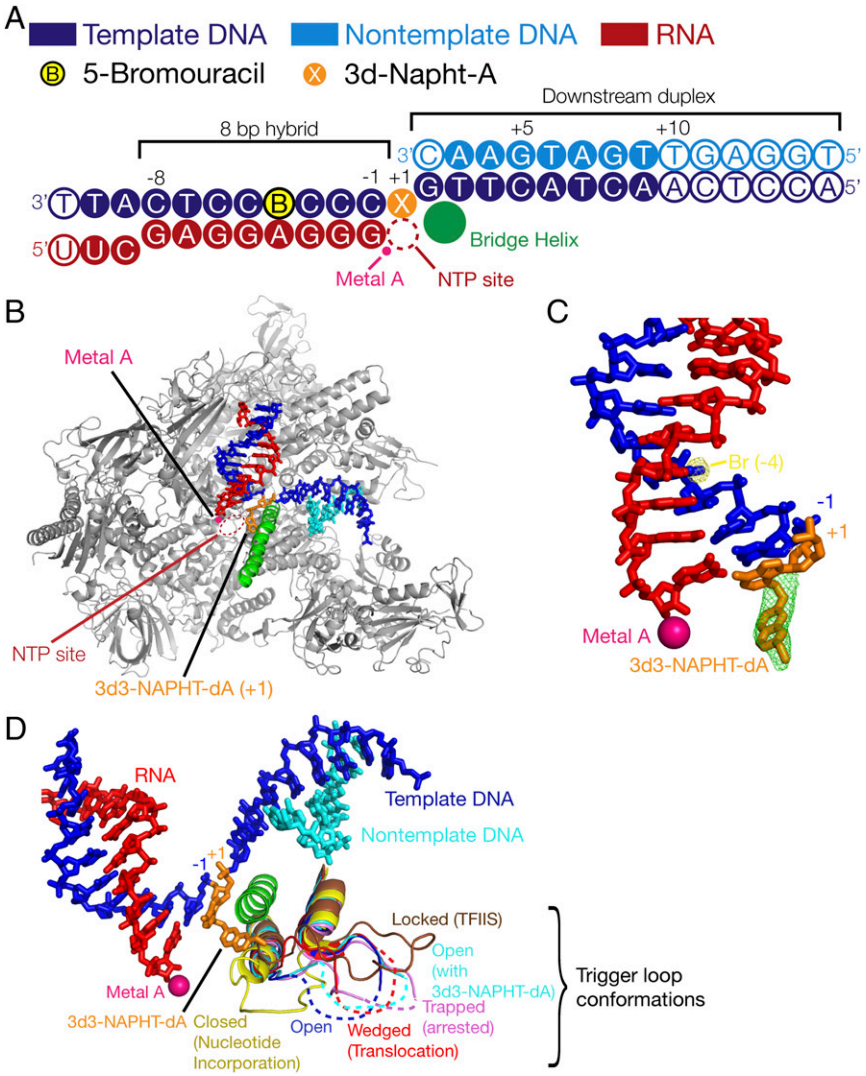

Fig. 4. Structure of a Pol II EC in the presence of 3d-Napht-A in the +1 site. The 12-subunit Pol II (4.1 mg/mL) was incubated with a 1.5-fold molar excess of nucleic acid scaffold containing the 3d-Napht-A analog and 5-Br-U. The sample was incubated for 20 min on ice before crystallization by hanging-drop vapor diffusion using as reservoir solution 4–7% PEG 6000, 200 mM ammonium acetate, 300 mM sodium acetate, 50 mM Hepes, pH 7.0, and 5 mM Tris(2-carboxyethyl)phosphine. Crystals were grown for 4–8 d, cryoprotected in mother solution supplemented with 22% glycerol and nucleic acid scaffold. Crystals were incubated overnight at 8 °C before they were harvested and flash-cooled in liquid nitrogen. (*A*) The nucleic acid scaffold used in the crystal structure is depicted schematically with respect to the +1 site containing the 3d-Napht-A base modification. The color scheme is used throughout the figure. (*B*) Overview of the Pol II EC structure with the modified adenine present in the +1 site, the nucleotide addition site. Pol II is shown as a silver ribbon model in a side view. The bridge helix is colored in green. Nucleic acids are presented as stick models and 3d-Napht-A is highlighted in orange. (*C*) Simulated annealing omit map after removing the 3d-Napht moiety at the +1 site from the model ($F_o - F_C$ map, contoured at 3σ, positive density is colored in green). A peak in the anomalous difference Fourier map (density is colored in yellow, contoured at 6σ) reveals the exact position of the bromine atom at position −4, allowing unambiguous assignment of the posttranslocated state. (*D*) Trigger-loop conformation. Comparison of the conformation of the trigger loop observed here (cyan) with alternative conformations observed previously for Pol II. The closed trigger loop (PDB ID code 2E2H), open trigger loop in the posttranslocation state (PDB ID code 1Y1W), wedged trigger loop (PDB ID code 2VUM), trapped trigger loop (PDB ID code 3PO2), and locked trigger loop (PDB ID code 3PO3) are depicted in yellow, blue, red, violet, and brown, respectively. Metal A is shown as a magenta sphere.

end of the DNA–RNA hybrid (Fig. 4*B*). The register of nucleic acids was unambiguously defined by bromine labeling of the DNA template strand at position −4 and anomalous diffraction (Fig. 4*C*). The DNA modification was clearly observed in the electron density (Fig. 4*C*). The structure was refined to a free R factor of 22% at a resolution of 3.2 Å, resulting in an atomic model with very good stereochemistry (Table S1).

The structure revealed a previously unobserved mode of Pol II interaction with a modified DNA nucleotide. The EC adopts the posttranslocation state with the modified adenine base being accommodated in the templating position opposite the +1 site that binds the nucleoside triphosphate substrate (Fig. 4*B*). The 3-deaza-3-methoxynaphtylethyl group contacts the central bridge helix in the Pol II active center from underneath. In particular, the second aromatic ring of 3d-Napht-A forms van der Waals contacts with the side-chain methyl group of bridge helix residue Thr831. The trigger loop adopts an open conformation, similar to that observed in a previous EC structure that adopts the posttranslocation state [Protein Data Bank (PDB) ID code 1Y1W].

The structure immediately suggests the mechanism of impaired Pol II progression and stalling at an alkylated template base and explains the structure-activity profiles observed herein. Superposition of a Pol II EC structure containing a closed trigger loop (PDB ID code 2E2H) (38) showed that the closed state cannot be accommodated in the presence of the alkylated nucleotide due to clashes between trigger loop residues Thr1080 and Leu1081 and the 3-deaza-3-methoxynaphtylethyl group (Fig. 4*D*). Inefficient nucleotide incorporation can apparently still take place, because catalysis can occur in a trigger loop-independent, low-fidelity fashion (39), explaining the observed misincorporations. After a single (mis)incorporation event translocation is strongly impaired, however, as this would result in major clashes of the 3d-Napht-A moiety with Pol II residues that very intimately interact with the minor groove of the hybrid base pair in the posttranslocation position −1. In addition, movement of the bridge helix, also required for translocation (40), is likely impaired by the observed alkyl-bridge helix contact.

Discussion

Here we report on the mechanism of Pol II stalling in response to minor-groove DNA alkylation relevant to minor-groove-alkylating anticancer agents. A reduction in RNA synthesis was observed when cancer cells were treated with the drug HMAF but not when treated with a methylating agent, suggesting the capacity of the minor-groove HMAF modification, but not a methyl group, to stall RNA Pol II. Thus, RNA extension reactions were performed with DNA constructs containing stable synthetic analogs that model drug alkylation products, an approach that overcomes the limitation of chemical instability that has precluded previous detailed evaluation of such modification. The large analog 3d-Napht-A,

corresponding to the main adduct from HMAF, was found to block the progress of Pol II after insertion of a nucleotide (Fig. 2*B*). The rate of UMP incorporation was reduced, with background CMP misincorporation being maintained (Fig. 3*A*). Moreover, further extension of RNA primers was completely inhibited. Finally, structural studies indicated that the mechanism of stalling differs from those defined previously at other DNA lesions, revealing a combination of interactions with the base pair at position −1 and the second ring of the modification with the trigger loop of RNA Pol II as the basis.

TC-NER–deficient cells have increased sensitivity to AFs, suggesting the capacity of the adducts to stall transcription (4–6). HMAF exposure of SW480 cells overexpressing PTGR1 led to a significant reduction in RNA synthesis capacity, consistent with previous observations concerning reduced RNA synthesis in human leukemia and HeLa cells, as well as increased degradation of stalled Pol II (4, 13, 41). Moreover, we found that the methylating agent MMS did not reduce RNA synthesis in cells (Fig. S2), consistent with the observation of transcription over 3d-Me-A (42). While MMS does not form 3-Me-A exclusively, its toxicity is mainly attributed to this adduct, and the use of an extremely high MMS dose (i.e., 500 μM) still led to no reduction in RNA synthesis. The 3-Me-A adduct is also formed by the minor-groove-binding drug methyl lexitropsin, for which higher drug sensitivity was observed in human glioma cells deficient in BER rather than TC-NER (43–46).

The stalling of isolated Pol II at 3d-Napht-A observed in this study supports the assertion that in cells treated with AFs transcription is stalled and the stalled Pol II initiates TC-NER and reduces drug action. The chemical basis of this cellular process appears to be associated with the alkyl adduct preventing translocation of the nascent +1 base pair to the next template position due to clashes with Pol II residues binding the minor-groove edge of the DNA–RNA base pair at position −1, and by a clash of the second ring on the methoxynaphtyl group with two residues of the mobile trigger loop (Fig. 4). These interactions highlight a different Pol II stalling mechanism than predicted by Xu et al. (33) in the case of polyamide minor-groove-binding agents, wherein Pol II was stalled upstream of the polyamide-bound DNA by interactions between the Switch 1 region and the minor-groove binder impeding translocation. The structure analysis and structure-activity relationships elucidated in the current study suggest the smaller phenethyl group of 3d-Phen-A does not prevent the trigger loop from closing, allowing Pol II to bypass analogs with only one aromatic ring. Finally, Pol II preferentially incorporated UMP opposite the smaller analogs 3d-Me-A and 3d-Phen-A, and RNA could be extended.

The mechanism of Pol II stalling reported herein should inform the design of improved anticancer alkylating agents that inhibit DNA synthesis without impeding the progression of RNA polymerase, thus evading TC-NER. Based on our results, 3-adenosine adducts with only one ring are tolerated by Pol II but do block the replicative DNA polymerase hPol α (16). Moreover, the chemical modifications did not destabilize DNA duplexes, suggesting that 3-AF-A adducts do not induce helix distortion and evade GG-NER (16). Thus, 3-adenosine adducts containing one phenyl ring may have a desired balance of properties to inhibit DNA replication but avoid TC-NER. The detailed insight derived from this study reveals how clashes between DNA adducts and residues binding the DNA–RNA minor-groove edge and the mobile trigger loop of RNA Pol II prevent translocation after insertion of a nucleotide opposite an adduct. Knowledge concerning structural characteristics that impede Pol II improves our understanding of how cells initiate the repair of damaged DNA and may also support the design of more effective cancer therapeutics.

Materials and Methods

Materials. Chemicals, reagents, and electrophoresis supplies were from Sigma-Aldrich and Bio-Rad Laboratories. Phosphoramidites of natural nucleosides and 3-deaza-3-methyl-adenine were purchased from Glen Research. Phosphoramidites of 3-deaza-3-phenethyl-adenine and 3-deaza-3-methoxynaphthalenethyl-adenine were synthesized as described previously (16). Unmodified DNA oligonucleotides and fluorescein-labeled RNA primers were obtained from VBC Biotech. The transcription buffer was 20 mM Hepes, pH 7.6, 60 mM $(NH_4)_2SO_4$, 8 mM $MgSO_4$, 10 μM $ZnCl_2$, 10% glycerol, and 10 mM DTT. SW480 cells overexpressing PTGR1 were obtained as previously described (11).

RNA Synthesis Recovery. Cells seeded at a density of 18,000 cells per well were washed twice with PBS solution (Gibco) and incubated with HMAF (0.5, 1 μM final concentration, in 0.1% DMSO medium), MMS (1, 500 μM final concentration, in 0.1% DMSO medium), or in 0.1% DMSO medium as negative control for 6 h at 37 °C. Transcription activity was evaluated with an RNA synthesis recovery assay (RRS) adapted from a previously published procedure (16). Full experimental details concerning cell culture conditions and RRS analysis appear in *Supporting Information*.

Synthesis of Oligonucleotides Containing 3-Deaza-3-Alkyl-Adenosine Adducts. Modified oligonucleotides were synthesized by solid phase on a Mermade 4 DNA synthesizer (Bioautomation). DNA templates for Pol II primer extension reactions were a 26-mer (5′-ACCTCAACTACTTG**A**CCCTCCTCATT-3′) and a 34-mer (5′- GCTGTTCACCG**A**GGTCCCTCTCGATGGC**T**GTAAGT-3′), adapted from previous studies (36). Synthesized oligonucleotides were purified by HPLC (Agilent 1100 Series) using an Agilent Luna 25-mm C18 column. The chromatographic mobile phases were 50 mM triethylammonium acetate and acetonitrile (ACN) and the gradient used was 10–15% ACN over 35 min. The eluted fractions containing DNA templates were concentrated to dryness in a MiVac centrifugal evaporator, resuspended in 100 μL deionized water, and checked for purity by direct injection into an Agilent MSD SL ion trap mass spectrometer with electrospray ionization.

Transcription with Pol II. Yeast Pol II was purified as described previously (24). Transcription reactions were performed with DNA scaffolds composed of a 26-mer DNA template containing Ade or modified Ade at the position indicated with an underline (5′-ACCTCAACTACTTG**A**CCCTCCTCATT-3′), a 14-mer nontemplate DNA (VBC Biotech) (5′-CAAGTAGTTGAGGT-3′), and an 11-mer RNA primer labeled with fluorescein at the 5′ end (FAM-5′-UUCGAGGAGGG-3′). Oligonucleotides (final concentration 11 μM for template and nontemplate DNA; 10 μM for RNA primer) were annealed by heating to 90 °C in Tris-EDTA buffer with 50 mM NaCl and allowed to slowly cool to 25 °C. ECs were formed by incubating 5 pmol Pol II with 10 pmol DNA scaffold at 20 °C for 20 min in the transcription buffer (total volume 10 μL). Transcription reactions were initiated by adding NTPs (1 μL, 10 mM). Reactions were allowed to proceed for 20 min then quenched by addition of aqueous EDTA (5 μL, 50 mM). For steady-state kinetic evaluation, reactions were performed at varying time points (between 0 and 60 min). The formation of extended primers was monitored by denaturing gel electrophoresis (7 M urea, 20% acrylamide) followed by visualization with Molecular Imager Gel Doc XR+Imaging System (Bio-Rad). Gel band intensities were quantified with ImageJ Lab 3.0. Percentage of primer extension were calculated with the equation $\sum I_{(n+x)}/(\sum I_{(n+x)} + I_n)$, where $I_{(n+x)}$ represents the intensity of all bands above the primer and I_n represents the band intensity of the nonextended primer. The twofold molar excess of DNA scaffold compared with the enzyme leaves a theoretical 50% unbound portion of primers unprocessed, and these residual RNA primers were used as an internal reference band. Values from kinetics experiments were plotted using GraphPad Prism and nonlinear regression analysis was carried out using the equation $Y = Y_m * (1 - e^{(-k*X)})$, where Y_m is the percentage of product formed, k is the apparent reaction rate, and X is time.

Pol II bypass of DNA adducts placed four bases downstream transcription start was performed with ECs composed of a 34-mer DNA template (5′-GCTGTTCACCG**A**GTCCCTCTCGATGGCTGTAAGT-3′), a 34-mer nontemplate DNA (5′-ACTTACA**G**CCATCGAGAGGGACTCGGTGAACAGC-3′), and a 9-mer RNA primer labeled with fluorescein at the 5′ end (5′-AUGGAGAGG-3′). ECs were assembled as described previously (24). The transcription reaction was performed at 37 °C and initiated by addition of NTPs (10 mM, 1 μL). After 30 min, the reaction was quenched with addition of EDTA solution (50 mM, 5 μL).

Crystal Structure Analysis. Twelve-subunit Pol II was complexed with a nucleic acid scaffold containing the 3d-Napht-A analog and 5-Br-U as described in the legend for Fig. 4. Diffraction data were collected at beamline X06SA of the Swiss Light Source at the Paul Scherrer Institut or beamline P13 at the Deutsches Elektronensynchrotron. The native dataset was collected at a wavelength of 0.976 Å. The Bromine peak dataset was collected at a wavelength of 0.919 Å. Diffraction images were processed with XDS (47). The

structure was solved with molecular replacement using a 12-subunit Pol II structure (PDB ID code 3HOX) without nucleic acids. Refinement was performed using Phenix.Refine (48). Refinement statistics are summarized in Table S1. The final model was analyzed using MolProbity (49). Ninety-two percent of residues were in Ramchandran plot favored regions, 7.1% in 752 allowed regions; 0.9% Ramachandran outliers were observed. Figures were generated using PyMOL (50).

ACKNOWLEDGMENTS. We thank Hauke Hillen, Kayo Nozawa, and Seychelle M. Vos for help with data collection and processing; Thomas Schulz for yeast fermentations; and Carina Burzinski for help with Pol II purification. This work was supported by Deutsche Forschungsgemeinschaft Grants SFB860 and SPP1935, European Research Council Advanced Investigator Grant TRANSREGULON 693023, and the Volkswagen Foundation (all to P.C.) and European Research Council Grant 260341 and Swiss National Science Foundation Grant 156280 (both to S.J.S.).

1. Salehan MR, Morse HR (2013) DNA damage repair and tolerance: A role in chemotherapeutic drug resistance. *Br J Biomed Sci* 70:31–40.
2. Cirauqui B, et al. (2016) DNA repair pathways to regulate response to chemoradiotherapy in patients with locally advanced head and neck cancer. *Tumour Biol* 37: 13435–13443.
3. Yu WK, et al. (2017) Chemoresistant lung cancer stem cells display high DNA repair capability to remove cisplatin-induced DNA damage. *Br J Pharmacol* 174: 302–313.
4. Jaspers NG, et al. (2002) Anti-tumour compounds illudin S and Irofulven induce DNA lesions ignored by global repair and exclusively processed by transcription- and replication-coupled repair pathways. *DNA Repair (Amst)* 1:1027–1038.
5. Koeppel F, et al. (2004) Irofulven cytotoxicity depends on transcription-coupled nucleotide excision repair and is correlated with XPG expression in solid tumor cells. *Clin Cancer Res* 10:5604–5613.
6. Otto C, et al. (2017) Modulation of cytotoxicity by transcription-coupled nucleotide excision repair is independent of the requirement for bioactivation of acylfulvene. *Chem Res Toxicol* 30:769–776.
7. Gong J, et al. (2007) Depurinating acylfulvene-DNA adducts: Characterizing cellular chemical reactions of a selective antitumor agent. *J Am Chem Soc* 129: 2101–2111.
8. Hargrove AE, et al. (2015) Tumor repression of VCaP xenografts by a pyrrole-imidazole polyamide. *PLoS One* 10:e0143161.
9. Anonymous (May 29, 2015) Oncology Venture, MPI's drug development arm and Lantern Pharma receive ICIP grant to advance Irofulven for metastatic prostate cancer. Available at https://globenewswire.com/news-release/2015/03/04/712201/10123208/en/Oncology-Venture-MPI-s-drug-development-arm-and-Lantern-Pharma-receive-ICIP-grant-to-advance-Irofulven-for-metastatic-prostate-cancer.html. Accessed July 10, 2016.
10. Neels JF, Gong J, Yu X, Sturla SJ (2007) Quantitative correlation of drug bioactivation and deoxyadenosine alkylation by acylfulvene. *Chem Res Toxicol* 20:1513–1519.
11. Pietsch KE, van Midwoud PM, Villalta PW, Sturla SJ (2013) Quantification of acylfulvene- and illudin S-DNA adducts in cells with variable bioactivation capacities. *Chem Res Toxicol* 26:146–155.
12. van Midwoud PM, Sturla SJ (2013) Improved efficacy of acylfulvene in colon cancer cells when combined with a nuclear excision repair inhibitor. *Chem Res Toxicol* 26: 1674–1682.
13. Woynarowski JM, et al. (1997) Effects on DNA integrity and apoptosis induction by a novel antitumor sesquiterpene drug, 6-hydroxymethylacylfulvene (HMAF, MGI 114). *Biochem Pharmacol* 54:1181–1193.
14. Hanawalt PC (2002) Subpathways of nucleotide excision repair and their regulation. *Oncogene* 21:8949–8956.
15. Glatt H, Pietsch KE, Sturla SJ, Meinl W (2014) Sulfotransferase-independent genotoxicity of illudin S and its acylfulvene derivatives in bacterial and mammalian cells. *Arch Toxicol* 88:161–169.
16. Malvezzi S, Angelov T, Sturla SJ (2017) Minor groove 3-Deaza-Adenosine analogues: Synthesis and bypass in translesion DNA synthesis. *Chemistry* 23:1101–1109.
17. Jiang H, Yang LY (1999) Cell cycle checkpoint abrogator UCN-01 inhibits DNA repair: Association with attenuation of the interaction of XPA and ERCC1 nucleotide excision repair proteins. *Cancer Res* 59:4529–4534.
18. Ljungman M, Lane DP (2004) Transcription–Guarding the genome by sensing DNA damage. *Nat Rev Cancer* 4:727–737.
19. Dimitri A, Burns JA, Broyde S, Scicchitano DA (2008) Transcription elongation past O6-methylguanine by human RNA polymerase II and bacteriophage T7 RNA polymerase. *Nucleic Acids Res* 36:6459–6471.
20. Tornaletti S, Maeda LS, Kolodner RD, Hanawalt PC (2004) Effect of 8-oxoguanine on transcription elongation by T7 RNA polymerase and mammalian RNA polymerase II. *DNA Repair (Amst)* 3:483–494.
21. You C, et al. (2012) A quantitative assay for assessing the effects of DNA lesions on transcription. *Nat Chem Biol* 8:817–822.
22. You C, Wang J, Dai X, Wang Y (2015) Transcriptional inhibition and mutagenesis induced by N-nitroso compound-derived carboxymethylated thymidine adducts in DNA. *Nucleic Acids Res* 43:1012–1018.
23. Brueckner F, Hennecke U, Carell T, Cramer P (2007) CPD damage recognition by transcribing RNA polymerase II. *Science* 315:859–862.
24. Damsma GE, Alt A, Brueckner F, Carell T, Cramer P (2007) Mechanism of transcriptional stalling at cisplatin-damaged DNA. *Nat Struct Mol Biol* 14:1127–1133.
25. Walmacq C, et al. (2015) Mechanism of RNA polymerase II bypass of oxidative cyclopurine DNA lesions. *Proc Natl Acad Sci USA* 112:E410–E419.
26. Wang D, Zhu G, Huang X, Lippard SJ (2010) X-ray structure and mechanism of RNA polymerase II stalled at an antineoplastic monofunctional platinum-DNA adduct. *Proc Natl Acad Sci USA* 107:9584–9589.
27. Shin JH, Xu L, Wang D (2017) Mechanism of transcription-coupled DNA modification recognition. *Cell Biosci* 7:9.
28. Shin JH, Xu L, Wang D (2016) RNA polymerase II acts as a selective sensor for DNA lesions and endogenous DNA modifications. *Transcription* 7:57–62.
29. Xu L, et al. (2014) Dissecting the chemical interactions and substrate structural signatures governing RNA polymerase II trigger loop closure by synthetic nucleic acid analogues. *Nucleic Acids Res* 42:5863–5870.
30. Fouqueau T, Zeller ME, Cheung AC, Cramer P, Thomm M (2013) The RNA polymerase trigger loop functions in all three phases of the transcription cycle. *Nucleic Acids Res* 41:7048–7059.
31. Brueckner F, Ortiz J, Cramer P (2009) A movie of the RNA polymerase nucleotide addition cycle. *Curr Opin Struct Biol* 19:294–299.
32. Da LT, et al. (2016) Bridge helix bending promotes RNA polymerase II backtracking through a critical and conserved threonine residue. *Nat Commun* 7:11244.
33. Xu L, et al. (2016) RNA polymerase II senses obstruction in the DNA minor groove via a conserved sensor motif. *Proc Natl Acad Sci USA* 113:12426–12431.
34. Beranek DT (1990) Distribution of methyl and ethyl adducts following alkylation with monofunctional alkylating agents. *Mutat Res* 231:11–30.
35. Brink A, Schulz B, Stopper H, Lutz WK (2007) Biological significance of DNA adducts investigated by simultaneous analysis of different endpoints of genotoxicity in L5178Y mouse lymphoma cells treated with methyl methanesulfonate. *Mutat Res* 625:94–101.
36. Gaykalova DA, Kulaeva OI, Pestov NA, Hsieh FK, Studitsky VM (2012) Experimental analysis of the mechanism of chromatin remodeling by RNA polymerase II. *Methods Enzymol* 512:293–314.
37. Burns JA, Dreij K, Cartularo L, Scicchitano DA (2010) O6-methylguanine induces altered proteins at the level of transcription in human cells. *Nucleic Acids Res* 38: 8178–8187.
38. Wang D, Bushnell DA, Westover KD, Kaplan CD, Kornberg RD (2006) Structural basis of transcription: Role of the trigger loop in substrate specificity and catalysis. *Cell* 127: 941–954.
39. Toulokhonov I, Zhang J, Palangat M, Landick R (2007) A central role of the RNA polymerase trigger loop in active-site rearrangement during transcriptional pausing. *Mol Cell* 27:406–419.
40. Brueckner F, Cramer P (2008) Structural basis of transcription inhibition by alpha-amanitin and implications for RNA polymerase II translocation. *Nat Struct Mol Biol* 15: 811–818.
41. Escargueil AE, et al. (2008) Influence of irofulven, a transcription-coupled repair-specific antitumor agent, on RNA polymerase activity, stability and dynamics in living mammalian cells. *J Cell Sci* 121:1275–1283.
42. Monti P, et al. (2011) 3-Methyl-3-deazaadenine, a stable isostere of N3-methyl-adenine, is efficiently bypassed by replication in vivo and by transcription in vitro. *DNA Repair (Amst)* 10:861–868.
43. Sweet JM, Carda B, Small GD (1981) Repair of 3-methyladenine and 7-methylguanine in nuclear DNA of Chlamydomonas: Requirement for protein synthesis. *Mutat Res* 84: 73–82.
44. Metz AH, Hollis T, Eichman BF (2007) DNA damage recognition and repair by 3-methyladenine DNA glycosylase I (TAG). *EMBO J* 26:2411–2420.
45. Bobola MS, Kolstoe DD, Blank A, Chamberlain MC, Silber JR (2012) Repair of 3-methyladenine and abasic sites by base excision repair mediates glioblastoma resistance to temozolomide. *Front Oncol* 2:176.
46. Bobola MS, et al. (2007) Human glioma cell sensitivity to the sequence-specific alkylating agent methyl-lexitropsin. *Clin Cancer Res* 13:612–620.
47. Kabsch W (2010) Xds. *Acta Crystallogr D Biol Crystallogr* 66:125–132.
48. Adams PD, et al. (2010) PHENIX: A comprehensive Python-based system for macromolecular structure solution. *Acta Crystallogr D Biol Crystallogr* 66:213–221.
49. Chen VB, et al. (2010) MolProbity: All-atom structure validation for macromolecular crystallography. *Acta Crystallogr D Biol Crystallogr* 66:12–21.
50. Schrödinger LLC (2015) The PyMOL Molecular Graphics System, version 1.8 (Schrödinger, LLC, New York).